


Article

Magnesium Oxybromides MOB-318 and MOB-518: Brominated Analogues of Magnesium Oxychlorides

Anna-Marie Lauermannová ¹, Michal Lojka ¹, Filip Antončík ¹, David Sedmidubský ¹,
Milena Pavlíková ², Zbyšek Pavlík ² and Ondřej Jankovský ^{1,*}

¹ Department of Inorganic Chemistry, Faculty of Chemical Technology, University of Chemistry and Technology, Technická 5, 166 28 Prague 6, Czech Republic; lauermaa@vscht.cz (A.-M.L.); michal.lojka@vscht.cz (M.L.); filip.antoncik@vscht.cz (F.A.); david.sedmidubsky@vscht.cz (D.S.)

² Department of Materials Engineering and Chemistry, Faculty of Civil Engineering, Czech Technical University in Prague, Thákurova 7, 166 29 Prague 6, Czech Republic; milena.pavlikova@fsv.cvut.cz (M.P.); pavlikz@fsv.cvut.cz (Z.P.)

* Correspondence: ondrej.jankovsky@vscht.cz; Tel.: +420-220442002

Received: 14 May 2020; Accepted: 9 June 2020; Published: 11 June 2020



Featured Application: The data acquired from the conducted tests and analyses can be used in the design and development of energy-efficient low-carbon construction materials. Because magnesium oxybromide phases (MOB-318, MOB-518) are stable, non-defective and well densified, high mechanical resistance of MOB-based materials can be anticipated similarly to magnesium oxychloride cement (MOC). Analogous to MOC, precipitated MOB phases can accommodate a great volume of inorganic and organic fillers and aggregates, which enables the production of alternative construction materials for specific applications. MOB-based materials can thus meet specific technical, functional and performance criteria of building practice. As MOB-318 can transmit light, it can be used in the design of a novel, highly optically-transparent material for light-transmitting decorative panels, partition walls, facing panels, translucent bricks and other architectural elements. Another specific attribute of MOB is its marble-like appearance, which makes it suitable as a decorative material. MOB-based composites can also serve as flame retardants. As such, they can potentially find use in the form of insulation boards or ceiling slabs to ensure the fire safety of steel structure buildings.

Abstract: The search for environmentally sustainable building materials is currently experiencing significant expansion. It is increasingly important to find new materials or reintroduce those that have been set aside to find a good replacement for Portland cement, which is widely used despite being environmentally insufficient and energy-intensive. Magnesium oxybromides, analogues to well-known magnesium oxychloride cements, fit both categories of new and reintroduced materials. In this contribution, two magnesium oxybromide phases were prepared and thoroughly analyzed. The stoichiometries of the prepared phases were $5\text{Mg}(\text{OH})_2 \cdot \text{MgBr}_2 \cdot 8\text{H}_2\text{O}$ and $3\text{Mg}(\text{OH})_2 \cdot \text{MgBr}_2 \cdot 8\text{H}_2\text{O}$. The phase analysis was determined using X-ray diffraction. The morphology was analyzed with scanning and transmission electron microscopy. The chemical composition was studied using X-ray fluorescence and energy dispersive spectroscopy. Fourier transform infrared spectroscopy was also used. The thermal stability and the mechanism of the release of gasses linked to the heating process, such as water and hydrobromic acid evaporation, were analyzed using simultaneous thermal analysis combined with mass spectroscopy. The obtained results were compared with the data available for magnesium oxychlorides.

Keywords: magnesium oxybromides; MOC; chemical and phase composition; morphology; FT-IR analysis; thermal stability

1. Introduction

In past decades, CO₂ production and other greenhouse gases (GHG) have grown rapidly, placing pressure on the industrial and manufacturing sectors to move towards environmental sustainability. In the construction industry, this tendency has manifested in the search for new materials that are less energy-intensive and produce a smaller amount of GHG compared to commonly used Portland cement (PC). The fabrication of 1 kg of PC leads to the production of approximately 0.81 kg CO₂. As PC is the most highly consumed human-made material, this ratio means it is responsible for roughly 5% of the world's production of GHG [1,2]. One of the possible answers to the search for alternative materials is magnesia-based cement and magnesium carbonates. The production of their precursors is less energy-consuming than the production of the precursors of PC, mostly because of the lower calcination temperature of MgCO₃ (preparation of caustic MgO occurs between 700 and 1000 °C, depending on the amount of impurities present in the precursor) compared to the calcination temperature of CaCO₃ (usually 900–1200 °C, sintering at 1450 °C). Additionally, reactive magnesia cement has the ability to absorb CO₂ from the atmosphere while forming various carbonates [3,4]. Chlorartinite formation in magnesium oxychloride cement (MOC) occurs upon exposure to gaseous CO₂ and coincides with an enhancement in water stability. Considering these two aspects, we can see it as a potentially CO₂-neutral, and therefore, eco-friendly material. Although magnesia-based binders have been known for over 150 years, they have been set aside because of the big upswing in the use of PC. However, they are now being rediscovered and studied again [5,6], not only due to the environmental aspects mentioned above but also due to their utility properties.

The application potential of magnesia-based building materials originates from their specific characteristics. Their low alkalinity (pH~10) makes them suitable for use with glass fibers as well as with a wide spectrum of aggregates [7] like tire rubber [8], fly ash [9] or wood particles [10,11]. Due to their elastic and acoustic properties, as well as their decorative appearance, these materials are also used in flooring [12,13], fire protective systems [14], decorative ivory-like structures [15], wall insulation [16], or grinding wheels [17]. Moreover, their curing time is relatively short, making such materials suitable for quick repairs. The kinetics of the formation of oxyhalides has been previously studied, showing that the curing time of these materials was much shorter than the curing time of regularly used PC [18–20].

Magnesium oxybromide cement (MOB) is similar to magnesium oxychloride cement, also known as MOC or Sorel cement, and was discovered in 1867 by Stanislas Sorel [21]. This material is a non-hydraulic binder obtained by mixing magnesium oxide powder with an aqueous solution of magnesium bromide in a specific ratio. As a non-hydraulic binder, MOB does not need humid conditions to cure.

The first evidence of magnesium oxybromides is dated to 1897, when they were discovered by Tasilly, who described them as a mixture of magnesium oxide and magnesium halide, considering their quantities compared to the amount of used water [22].

Magnesium oxychloride cement shows unique properties that are superior compared to Portland cement. Such properties include specific density, which is significantly lower with higher compressive and flexural strength, elevated fire resistance [23], good resistance to abrasion [24,25] and low thermal conductivity. It can thus be assumed that MOB provides a similar set of properties. Another specific advantage of MOB is its marble-like appearance, which makes it suitable as a decorative material.

Another similarity between MOC and MOB are the phase relations in the MgO-MgX₂-H₂O system. The phases known in the MgO-MgCl₂-H₂O system, named according to the ratio of the input compounds, are Phase 2 (2MgO·MgCl₂·5H₂O) and 9 (9MgO·MgCl₂·4H₂O), which are formed at elevated temperatures, and Phase 3 (3MgO·MgCl₂·8H₂O) and Phase 5 (5MgO·MgCl₂·8H₂O) that exist at ambient temperature. The stoichiometry of Phases 3 and 5 in the MOB system is quite similar: 3MgO·MgBr₂·8H₂O and 5MgO·MgBr₂·8H₂O [26–28]. The structure of both phases is visualized in Figure 1. Phases in both MOB and MOC systems show similar microstructures. They are obtained in the form of needle-shaped crystals, and both are triclinic and isomorphous. Such microstructures result in very good mechanical properties [29,30]. In this paper, we prepared both of the above-mentioned

phases in the system MgO-MgBr₂-H₂O. We analyzed their structure and described their thermal behavior in detail. The drawings of crystal structures (Figure 1) were generated by VESTA software [31].

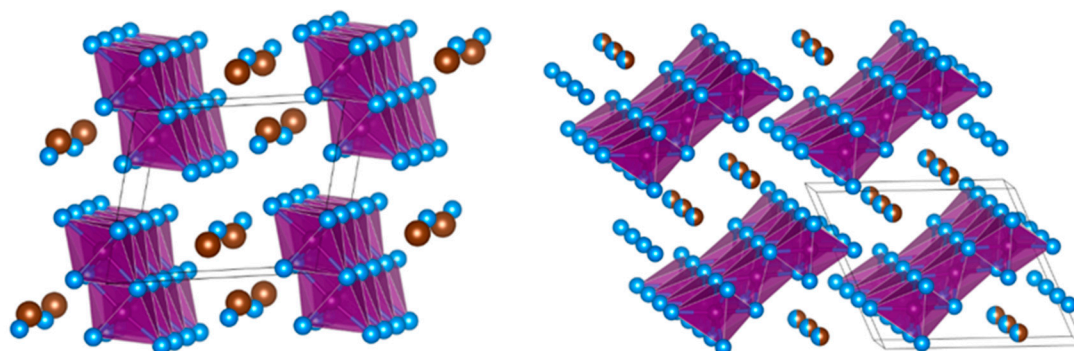


Figure 1. Crystal structures of magnesium oxybromide (MOB) phases MOB-318 (**left**) and MOB-518 (**right**). Mg atoms are located in the centers of the distorted octahedra formed by oxygen atoms. Br atoms are brown; O atoms are blue. Brown-blue spheres in the MOB-518 structure correspond to a mixed site occupied by bromide anions and water molecules (hydrogen atoms are not shown).

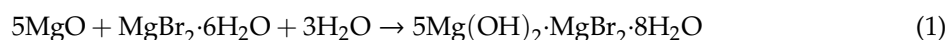
2. Materials and Methods

The following chemicals were used for the experiment: MgBr₂·6H₂O (>99%, PENTA, Prague, Czech Republic) and MgO (>98%, PENTA, Prague, Czech Republic). Deionized water (16.8 MΩ) was used for all syntheses. Both precursors were analyzed using X-ray fluorescence, confirming their high purity. The weight percentages of the elements (for MgO given on the basis of oxides) can be seen in Table 1.

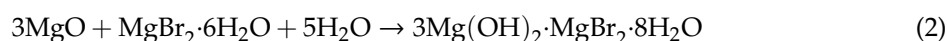
Table 1. Table of element percentages in the precursors obtained by XRF.

Element	Content in MgBr ₂ ·6H ₂ O (wt%)	Content in MgO (wt%)
Mg	11.44	99.19
P	0.01	-
Cl	0.10	0.38
Br	88.45	0.04
Ca	-	0.16
Al	-	0.13
S	-	0.10

The ratio 5 MgO to MgBr₂·6H₂O was used for synthesis of the stoichiometric phase of MOB with composition 5Mg(OH)₂·MgBr₂·8H₂O. To prepare the sample, 9.4 g of MgBr₂·6H₂O was dissolved in 4.1 g of deionized water in a plastic beaker. Next, 6.5 g of magnesium oxide was added, and the suspension was intensively stirred for 5 min. The following equation (Equation (1)) summarizes the formation of Phase 5:



Similarly, the stoichiometric phase 3Mg(OH)₂·MgBr₂·8H₂O was prepared using the ratio 3 MgO to MgCl₂·6H₂O to 5 H₂O. We dissolved 11.6 g of MgBr₂·6H₂O in 3.6 g of deionized water in a plastic beaker. In the next step, 4.8 g of magnesium oxide was added, and the suspension was intensively stirred for 5 min. The formation is summarized in the following equation (Equation (2)):



The phases magnesium bromide-trihydroxide tetrahydrate (stoichiometry $3\text{MgO}\cdot\text{MgBr}_2\cdot 8\text{H}_2\text{O}$ or $\text{Mg}_2(\text{OH})_3\text{Br}\cdot 4\text{H}_2\text{O}$) and magnesium bromide-pentahydroxide tetrahydrate (stoichiometry $5\text{MgO}\cdot\text{MgBr}_2\cdot 8\text{H}_2\text{O}$ or $\text{Mg}_3(\text{OH})_5\text{Br}\cdot 4\text{H}_2\text{O}$) are termed MOB-318 and MOB-518, respectively. Both prepared samples are shown in Figure 2.

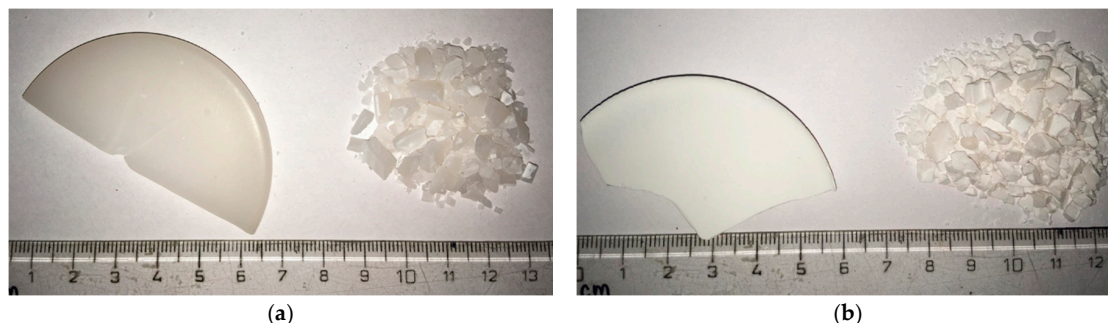


Figure 2. Samples (a) MOB-318, (b) MOB-518. The scale bar is in cm.

X-ray fluorescence analysis (XRF) was performed using an Axios sequential WD-XRF spectrometer (PANalytical, Almelo, Netherlands) equipped with an Rh anode end-window X-ray tube fitted with a $50\ \mu\text{m}$ beryllium window. The resulting data were collected by SuperQ software. The analyzed material was pressed, without any binding agent, onto H_3BO_3 pellets with a total thickness of approximately 5 mm and a diameter of 40 mm.

X-ray powder diffraction (XRD) was carried out by Bruker D2 Phaser, the powder diffractometer with Bragg–Brentano geometry, applying $\text{CuK}\alpha$ radiation ($\lambda = 0.15418\ \text{nm}$, $U = 30\ \text{kV}$, $I = 10\ \text{mA}$) and sample rotation (5 rounds per minute). The step size was set to 0.02025° (2θ), and the overall data were collected from the angular range of $5\text{--}80^\circ$. Measurements were performed after 5 weeks of curing.

Scanning electron microscopy (SEM) performed on a Tescan MAIA 3 was used for the study of surface morphology. The elemental composition and mapping were characterized using an energy dispersive spectroscopy (EDS) analyzer (X-Max150) with a $20\ \text{mm}^2$ SDD detector (Oxford Instruments, High Wycombe, UK) and AZtecEnergy software. The sample was put on a carbon conductive tape in order to ensure the conductivity of the experiments. For both SEM and SEM-EDS analysis, the electron beam was set to 10 kV, with 10 mm work distance.

High-resolution transmission electron microscopy (HR-TEM) was performed using an EFTEM Jeol 2200 FS microscope (Jeol, Tokyo, Japan). A 200 keV acceleration voltage was used for the measurement. Elemental maps and EDS spectra were acquired with an X-MaxN 80 TS SDD detector from Oxford Instruments (Oxfordshire, UK). The sample preparation was attained by drop-casting the suspension ($1\ \text{mg mL}^{-1}$ in water) on a TEM grid (Cu; 200 mesh; Formvar/carbon) and then drying in a vacuum dryer at $25\ ^\circ\text{C}$ and $p/p^0 = 0.2$.

Simultaneous thermal analysis combined with mass spectroscopy (STA-MS) was performed using the Setsys Evolution apparatus from Setaram in a temperature range up to $650\ ^\circ\text{C}$. The measurements were performed in a dynamic helium atmosphere with a flow rate of $50\ \text{mL/min}$ and a heating rate of $5\ ^\circ\text{C/min}$. An OmniStar mass spectrometer (MS) (Pfeiffer Vacuum GmbH, Aßlar, Germany) was used to analyze gases that evolved during the heating.

Fourier transform infrared (FT-IR) spectroscopy was used for the identification of chemical bonds in the hardened MOB samples. Mid-infrared spectra were analyzed on a Nicolet 6700 spectrometer (Thermo Fisher Scientific, Waltham, MA, USA), using the attenuated total reflectance (ATR) technique after 32 scans. The wavenumbers ranged from $4000\ \text{cm}^{-1}$ to $400\ \text{cm}^{-1}$, with the spectral resolution of $4\ \text{cm}^{-1}$. Samples were homogenized in an agate grinding mortar.

3. Results and Discussion

According to the reactions in Equations (1) and (2), two samples of MOB were prepared and then characterized. Firstly, the purity of both samples was determined using XRD (see Figure 3). This analysis was performed after five weeks of hardening, and showed a single-phase composition for both MOB-318 ($3\text{Mg}(\text{OH})_2 \cdot \text{MgBr}_2 \cdot 8\text{H}_2\text{O}$, ICDD 00-007-0411) and MOB-518 ($5\text{Mg}(\text{OH})_2 \cdot \text{MgBr}_2 \cdot 8\text{H}_2\text{O}$, ICDD 00-012-0121). As can be seen from both diffractograms, there was a strong background due to the amorphous nature of the samples. Some minor reflections in both diffractograms were present due to the hydroxycarbonates, which were formed on the MOB surface. Let us note that a slight discrepancy was found for 2θ positions of MOB-518 compared to the reference ICDD 00-012-0121.

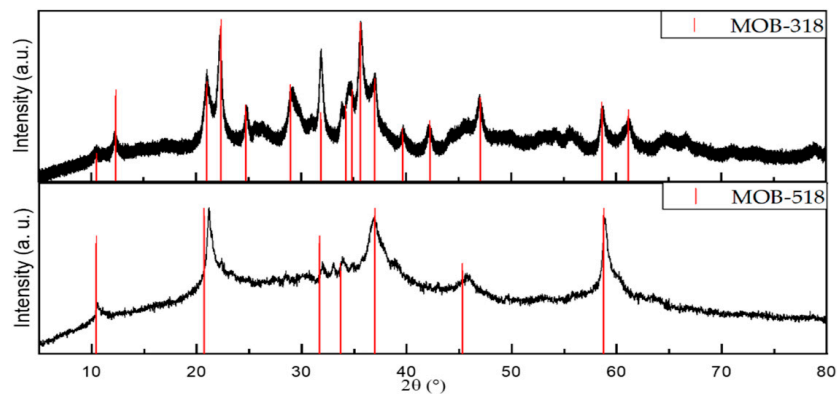


Figure 3. XRD patterns for MOB-318 and MOB-518 after five weeks.

SEM analysis was performed to study the microstructure, showing the typical needle-shaped crystals of both MOB phases (see Figure 4). The needles were visible at high magnification, with dimensions between 1 and 5 μm in length and approximately 0.5 μm in width. Overall, the samples were non-defective, and their structures held together very well.

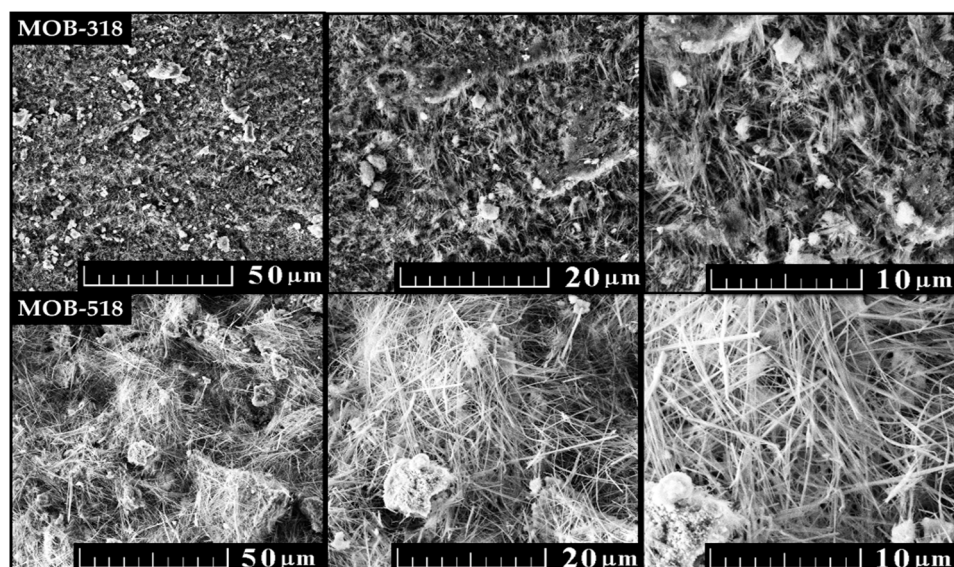


Figure 4. SEM micrographs of MOB-318 and MOB-518.

In the next step, EDS was used to determine the chemical composition of the samples. In both samples, magnesium, oxygen and bromine were detected, as well as a small amount of carbon. The presence of carbon was caused by the absorption of CO_2 from the atmosphere while forming magnesium carbonates. The results of the EDS can be seen in Figure 5. EDS maps confirmed a

homogenous distribution of detected elements which corresponded to the results obtained by XRD. Bromine content was slightly lower in sample MOB-518, which was in agreement with the composition of both phases.

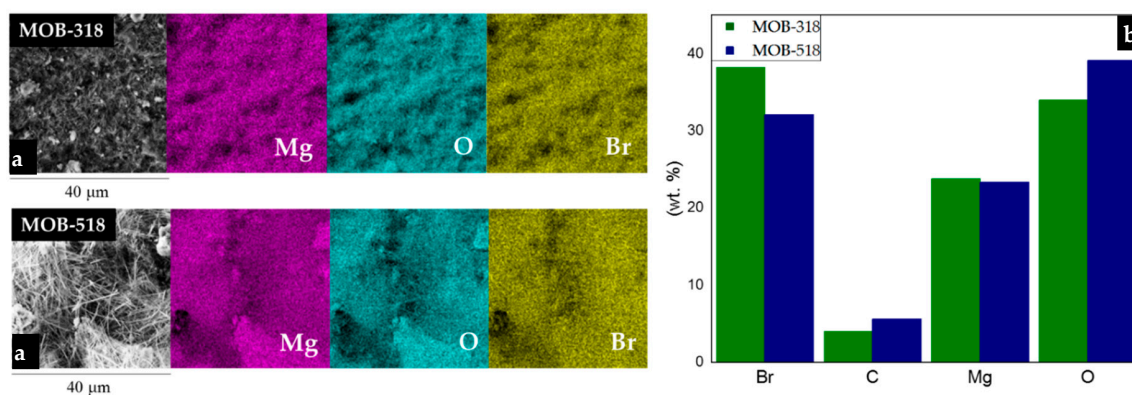


Figure 5. (a) Elemental maps of MOB-318 and MOB-518, (b) chemical composition obtained by EDS.

The shape and size of the individual MOB crystals was studied using TEM. The results showed a structure typical for magnesium oxychlorides. Additionally, the magnesium oxybromides had needle-like crystals that were approximately 1–5 μm long and less than 0.5 μm wide. The results are shown in Figure 6.

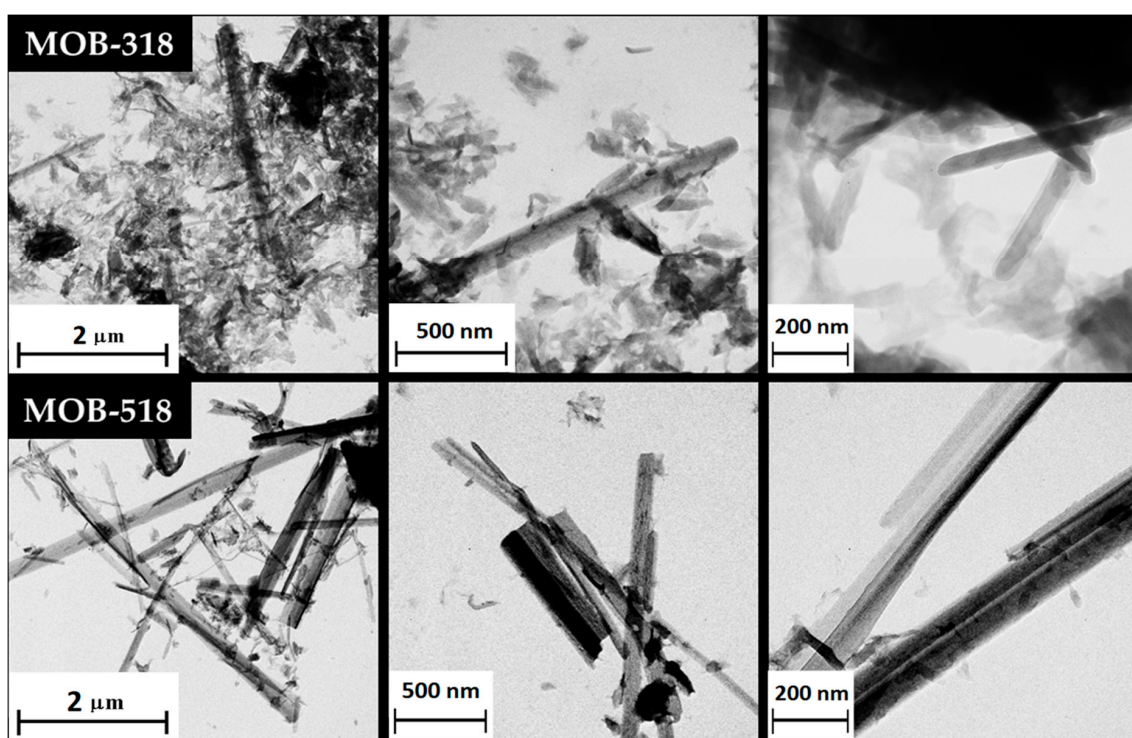


Figure 6. TEM micrographs of MOB-318 and MOB-518.

The collected FT-IR spectra (see Figure 7) of the tested magnesium oxybromide phases signed as MOB-318 and MOB-518 contain the bands arising from the fundamental vibrations of structural H₂O and the lattice vibrations of MgBr₂ and Mg(OH)₂ (Table 2). As originally reported by Shi et al. [32], the absorption bands near 1600 cm⁻¹ are associated with H₂O bending mode vibration; the bands in the range of 2000–3700 cm⁻¹ are caused by the symmetric and asymmetric stretching mode of O-H bonds in H₂O and Mg(OH)₂. The series of modes in the range of 1000–400 cm⁻¹ are the result of

the existence of lattice translation modes (Mg-OH) and vibrational modes of the lattice showing the Mg-O/Mg²⁺, O/O-Mg-O/O-Mg²⁺-O bonds [33]. The absorption band at 853 cm⁻¹ could be attributed to the characteristic absorption peak of cubic Mg-O. Lattice vibration modes of Mg-O/Mg-Br bonds were observed near 500 cm⁻¹ in the absorption spectrum. Translation vibrations of Mg/Mg-O and Mg-OH observed at about 500 cm⁻¹ were overlapped with strong deformation and stretching vibrations of Mg-Br. Let us note that the band at 1150 cm⁻¹ were visible due to the surface carbonation of both samples. This was further confirmed by STA-MS.

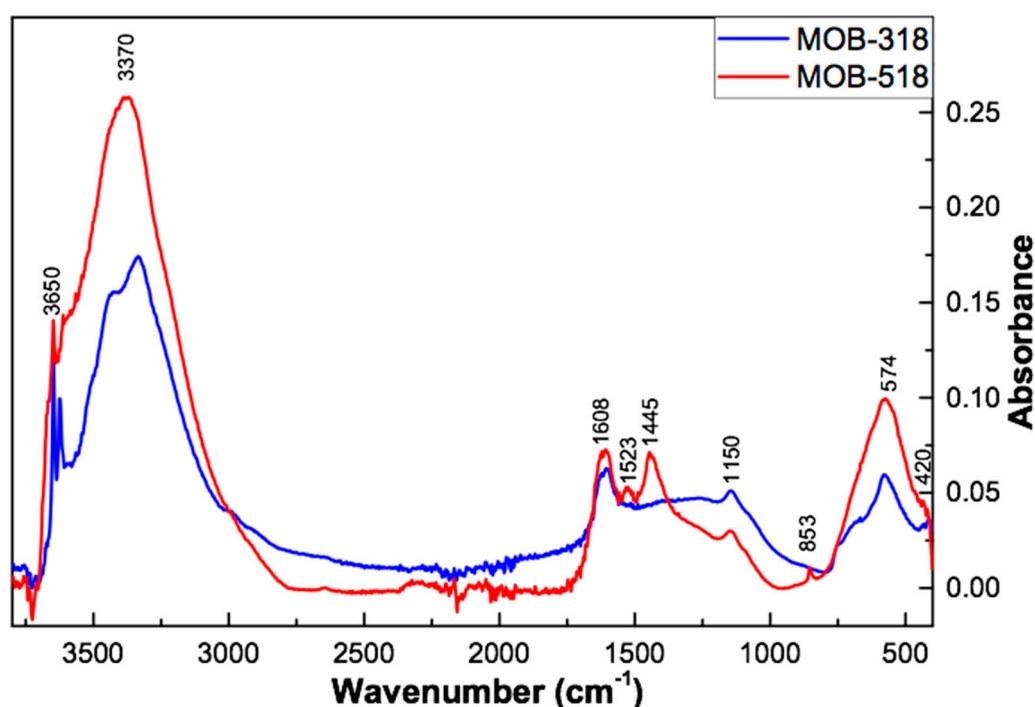
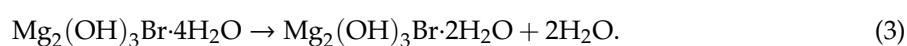


Figure 7. Collected FT-IR spectra of tested magnesium oxybromide phases.

Table 2. Assignments of the major absorption bands of MOB.

Wavenumbers (cm ⁻¹)	Assignment
3648, 3623	Stretching modes (ν) of O-H in Mg(OH) ₂
3370	Stretching modes (ν) of H-O-H in H ₂ O
2050	Bending (δ) and rocking (ρ) vibrations of H-O-H in H ₂ O
1608	Bending (δ) vibration of H-O-H in MgBr ₂ ·8H ₂ O
1523, 1445	Stretching modes (ν) of Mg-O MgBr ₂ ·8H ₂ O
853	Stretching vibration (ν) of Mg-O cubic structure
574	Deformation (δ) and stretching (ν) vibrations of Mg-Br
420	Vibrational modes of the lattice showing the Mg-O/Mg ²⁺ , O/O-Mg-O/O-Mg ²⁺ -O bonds

To determine the thermal stability of the samples, we used simultaneous thermal analysis combined with mass spectrometry (Figure 8). During the heating of the sample MOB-318, a number of thermal effects were observed. The first one began around ~90 °C and could be attributed to a release of two molecules of water. The reaction is summarized in Equation (3):



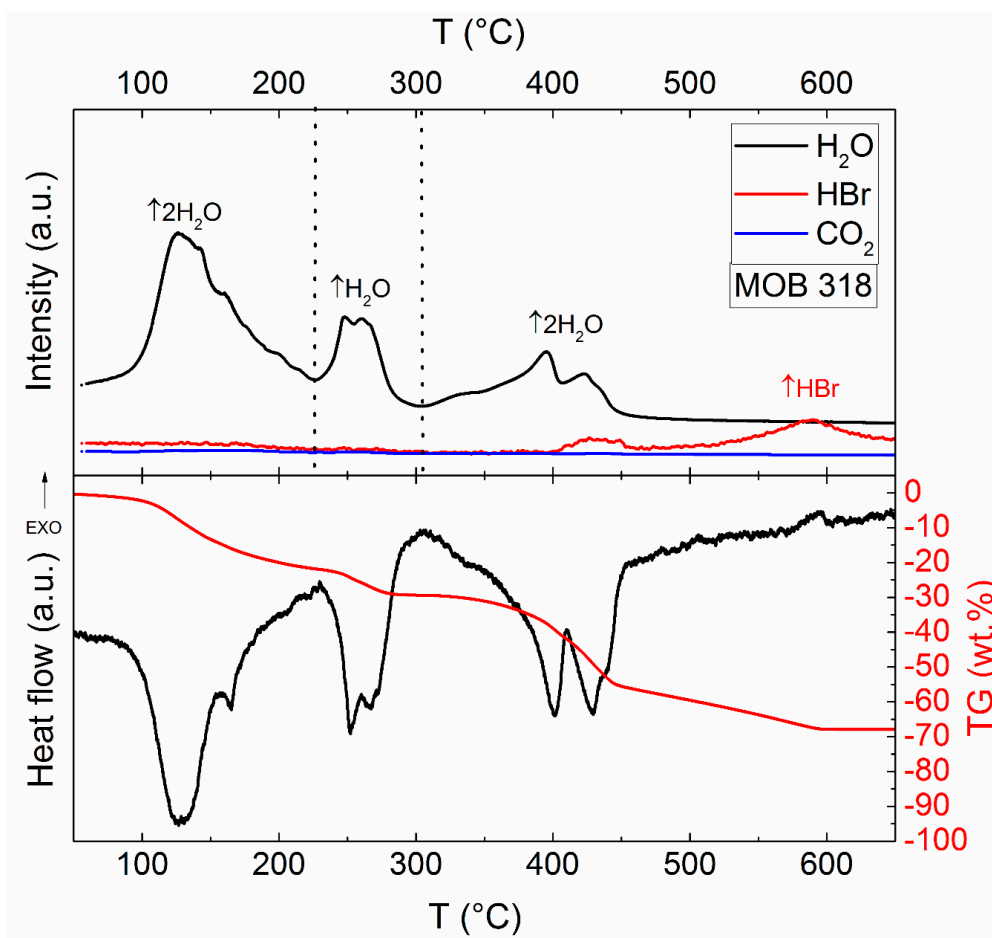
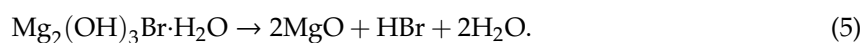


Figure 8. Simultaneous thermal analysis with mass spectroscopy of MOB-318 measured in an inert atmosphere.

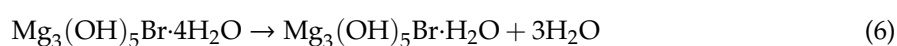
The next step was the second effect with a maximum at ~ 250 °C, which could be attributed to a release of one molecule of water (see Equation (4)):



The third endothermic effect beginning at ~ 380 °C was attributed to a release of two molecules of water, accompanied by a release of hydrobromic acid, which was evolving continuously at temperatures higher than 400 °C (see Equation (5)):



The thermal behavior of the sample MOB-518 is comparable to the thermal behavior of its chlorinated analogue, which has already been described in literature [34]. During the heating, five effects were detected from the heat flow signal (see Figure 9). The first endothermic effect was attributable to a release of three molecules of water (see Equation (6)) and its maximum was at ~ 125 °C.



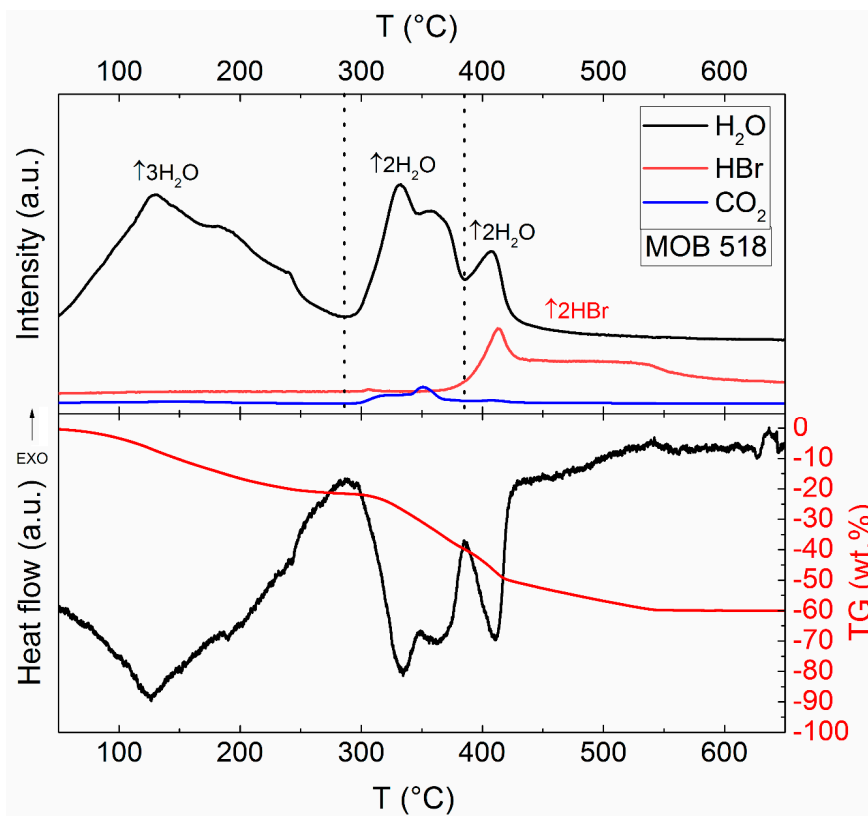
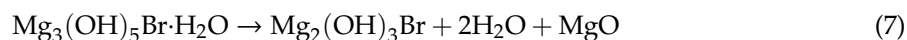
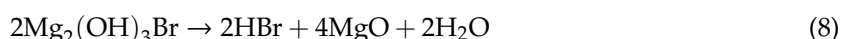


Figure 9. Simultaneous thermal analysis with mass spectrometry of MOB-518 measured in an inert atmosphere.

The next step of the heating showed another endothermic effect (with two local maxima at ~ 340 °C and 370 °C, respectively) which was attributed to the release of two water molecules (Equation (7)).



The last effect (maximum at ~ 420 °C) was attributed to a release of two crystalline water molecules and two hydrobromic acid molecules (see Equation (8)). After this step, only pure MgO was obtained.



We would like to note that during the heating of MOB-518, there was also a release of CO_2 around 350 °C caused by the decomposition of MgCO_3 that was formed on the sample surface. The process of formation of MgCO_3 on the surface of magnesia-based materials has previously been described in literature [35].

4. Conclusions

Ecologically sustainable building materials are increasingly important as the impacts of the global climate crisis become increasingly severe. Billions of tons of Portland cement are produced annually, inundating the atmosphere with massive amounts of CO_2 which is connected to the decomposition of precursors in cement production plants. In view of this, there is a growing interest in sustainable materials for construction use and developing low-energy and low-carbon alternatives to Portland cement with similar or better functional properties.

The main objective of this paper was to prepare and study stable MOB phases as alternative materials to Portland cement. The measurements results demonstrated that this binder was easy to prepare and CO_2 -neutral due to its ability to capture CO_2 from the atmosphere. This process not only

acted as an eco-friendly reaction, but also resulted in a more densified and mechanically resistant product. The results also displayed similarities between MOB and the already known MOC, showing their analogous structure, composition, properties and thermal stability. The collected mid-infrared spectra enabled the identification of fundamental vibrations of structural H₂O and lattice vibrations of MgBr₂ and Mg(OH)₂. The investigation of thermal stability showed the full process of decomposition of MOB, which was divided into several steps and spread across a temperature interval between 50 and 650 °C. Both MOB phases were continuously decomposed, and the final products of the process were magnesium oxide, water and hydrobromic acid for both phases, where both water and hydrobromic acid molecules were released in a gaseous form.

The application potential of the construction materials based on MOB lie in places with higher concentrations of CO₂, e.g., in areas with higher traffic or industrial air pollution. Using such materials in wall insulation or flooring can cause a reduction of CO₂ by forming carbonated MOB. In this way, the local concentration of CO₂ is lowered, making the environment cleaner and healthier to live and work in. The light-transmitting capacity of MOB-318 enables the development of a novel optically-transparent material for decorative purposes and specific architectural intentions, such as translucent partition walls and facing panels. Based on the identified thermal decomposition processes taking place in MOB materials at elevated temperatures, these materials can be applied as flame retardants and passive fire protection to reduce the fire hazard in buildings.

Author Contributions: Conceptualization, A.-M.L. and O.J.; methodology, O.J., M.P. and Z.P.; investigation, A.-M.L., M.L., F.A., O.J., D.S., M.P. and Z.P.; data curation, A.-M.L., M.P., O.J., D.S. and Z.P.; writing—original draft preparation, A.-M.L., M.P., O.J. and Z.P. All authors have read and agreed to the published version of the manuscript.

Funding: This research was funded by the Czech Science Foundation, grant number 19-00262S—Reactive magnesia cement-based composites with selected admixtures and additives.

Conflicts of Interest: The authors declare no conflict of interest.

References

1. Imbabi, M.S.; Carrigan, C.; McKenna, S. Trends and developments in green cement and concrete technology. *Int. J. Sustain. Built Environ.* **2012**, *1*, 194–216. [[CrossRef](#)]
2. Naik, T.R. Sustainability of Concrete Construction. *Pract. Period. Struct. Des. Constr.* **2008**, *13*, 98–103. [[CrossRef](#)]
3. Góchez, R.; Vreeland, T.; Wambaugh, J.; Kitchens, C.L. Conversion of magnesium oxychloride to chlorartinite and resulting increased water resistance. *Mater. Lett.* **2017**, *207*, 1–3. [[CrossRef](#)]
4. Power, I.M.; Dipple, G.; Francis, P. Assessing the carbon sequestration potential of magnesium oxychloride cement building materials. *Cem. Concr. Compos.* **2017**, *78*, 97–107. [[CrossRef](#)]
5. Harrison, J. Reactive Magnesium Oxide Cements. Patent WO 01/55049 A1, 2 August 2001.
6. Walling, S.; Provis, J.L. Magnesia-Based Cements: A Journey of 150 Years, and Cements for the Future? *Chem. Rev.* **2016**, *116*, 4170–4204. [[CrossRef](#)]
7. Liška, M.; Al-Tabbaa, A. Performance of magnesia cements in pressed masonry units with natural aggregates: Production parameters optimisation. *Constr. Build. Mater.* **2008**, *22*, 1789–1797. [[CrossRef](#)]
8. Biel, T.D.; Lee, H. Magnesium oxychloride cement concrete with recycled tire rubber. *Transp. Res. Rec.* **1996**, *1561*, 6–12. [[CrossRef](#)]
9. Li, Y.; Yu, H.; Zheng, L.; Wen, J.; Wu, C.; Tan, Y. Compressive strength of fly ash magnesium oxychloride cement containing granite wastes. *Constr. Build. Mater.* **2013**, *38*, 1–7. [[CrossRef](#)]
10. He, P.; Hossain, U.; Poon, C.S.; Tsang, D.C. Mechanical, durability and environmental aspects of magnesium oxychloride cement boards incorporating waste wood. *J. Clean. Prod.* **2019**, *207*, 391–399. [[CrossRef](#)]
11. Zhou, X.; Li, Z. Light-weight wood–magnesium oxychloride cement composite building products made by extrusion. *Constr. Build. Mater.* **2012**, *27*, 382–389. [[CrossRef](#)]
12. Plekhanova, T.; Kerienė, J.; Gailius, A.; Yakovlev, G.I. Structural, physical and mechanical properties of modified wood–magnesia composite. *Constr. Build. Mater.* **2007**, *21*, 1833–1838. [[CrossRef](#)]

13. Sugimoto, K.; Dinnebier, R.; Schlecht, T. Structure determination of $\text{Mg}_3(\text{OH})_5\text{Cl} \cdot 4\text{H}_2\text{O}$ (f5 phase) from laboratory powder diffraction data and its impact on the analysis of problematic magnesia floors. *Acta Crystallogr. Sect. B Struct. Sci.* **2008**, *63*, 805–811. [[CrossRef](#)] [[PubMed](#)]
14. Xia, S.; Xing, P.; Gao, S. Studies on the basic compounds of magnesia cement: The thermal behaviour of magnesium oxychlorides. *Thermochim. Acta* **1991**, *183*, 349–363. [[CrossRef](#)]
15. Maravelaki-Kalaitzaki, P.; Moraitou, G. Sorel's cement mortars: Decay susceptibility and effect on pentelic marble. *Cem. Concr. Res.* **1999**, *29*, 1929–1935. [[CrossRef](#)]
16. de Castellar, M.D.; Lorente, J.C.; Traveria, A.; Tura, J.M. Cracks in sorel's cement polishing bricks as a result of magnesium oxychloride carbonatation. *Cem. Concr. Res.* **1996**, *26*, 1199–1202. [[CrossRef](#)]
17. Montle, J.F.; Mayhan, K.G. The role of magnesium oxychloride as a fire-resistive material. *Fire Technol.* **1974**, *10*, 201–210. [[CrossRef](#)]
18. Lojka, M.; Jankovský, O.; Jiříčková, A.; Lauermannová, A.-M.; Antončík, F.; Sedmidubský, D.; Pavlík, Z.; Pavlíková, M. Thermal stability and kinetics of formation of magnesium oxychloride phase $3\text{Mg}(\text{OH})_2 \cdot \text{MgCl}_2 \cdot 8\text{H}_2\text{O}$. *Materials* **2020**, *13*, 767. [[CrossRef](#)]
19. Góchez, R.; Wambaugh, J.; Rochner, B.; Kitchens, C.L. Kinetic study of the magnesium oxychloride cement cure reaction. *J. Mater. Sci.* **2017**, *37*, 866–7646. [[CrossRef](#)]
20. Sglavo, V.M.; De Genua, F.; Conci, A.; Ceccato, R.; Cavallini, R. Influence of curing temperature on the evolution of magnesium oxychloride cement. *J. Mater. Sci.* **2011**, *46*, 6726–6733. [[CrossRef](#)]
21. Sorel, S. On a new magnesium cement. *C. R. Acad. Sci.* **1867**, *65*, 102–104.
22. Tasilly, E. Sels basiques de magnésium. *C. R. Acad. Sci.* **1897**, *125*, 605.
23. Thompson, H.C. Fireproof Product Using Magnesium Oxychloride Cement. U.S. Patent 3,963,849, 15 June 1976.
24. Li, G.; Yu, Y.; Li, J.; Wang, Y.; Liu, H. Experimental study on urban refuse/magnesium oxychloride cement compound floor tile. *Cem. Concr. Res.* **2003**, *33*, 1663–1668. [[CrossRef](#)]
25. Qiao, H.; Cheng, Q.; Wang, J.; Shi, Y. The application review of magnesium oxychloride cement. *J. Chem. Pharm. Res.* **2014**, *6*, 180–185.
26. Urwongse, L.; Sorrell, C.A. The system $\text{MgO}-\text{MgCl}_2-\text{H}_2\text{O}$ at 23 °C. *J. Am. Ceram. Soc.* **1980**, *63*, 501–504. [[CrossRef](#)]
27. Li, Z.; Chau, C. Influence of molar ratios on properties of magnesium oxychloride cement. *Cem. Concr. Res.* **2007**, *37*, 866–870. [[CrossRef](#)]
28. Dorrepaal, R.; Gowen, A. Identification of Magnesium Oxychloride Cement Biomaterial Heterogeneity using Raman Chemical Mapping and NIR Hyperspectral Chemical Imaging. *Sci. Rep.* **2018**, *8*, 13034. [[CrossRef](#)] [[PubMed](#)]
29. Matković, B.; Young, J.F. Microstructure of Magnesium Oxychloride Cements. *Nat. Phys. Sci.* **1973**, *246*, 79–80. [[CrossRef](#)]
30. De Wolff, P.M.; Walter-Lévy, L. The crystal structure of $\text{Mg}_2(\text{OH})_3(\text{Cl},\text{Br}) \cdot 4\text{H}_2\text{O}$. *Acta Crystallogr.* **1953**, *6*, 40–44. [[CrossRef](#)]
31. Momma, K.; Izumi, F. VESTA 3 for three-dimensional visualization of crystal, volumetric and morphology data. *J. Appl. Crystallogr.* **2011**, *44*, 1272–1276. [[CrossRef](#)]
32. Shi, E.; Wang, A.; Ling, Z. MIR, VNIR, NIR, and Raman spectra of magnesium chlorides with six hydration degrees: Implication for Mars and Europa. *J. Raman Spectrosc.* **2019**, 1–14. [[CrossRef](#)]
33. Sugimoto, K.; Dinnebier, R.E.; Hanson, J.C. Structures of three dehydration products of bischofite from in situ synchrotron powder diffraction data ($\text{MgCl}_2 \cdot n\text{H}_2\text{O}$; $n = 1, 2, 4$). *Acta Crystallogr. Sect. B Struct. Sci.* **2007**, *63*, 235–242. [[CrossRef](#)]
34. Jiříčková, A.; Lojka, M.; Lauermannová, A.-M.; Antončík, F.; Sedmidubský, D.; Pavlíková, M.; Záleská, M.; Pavlík, Z.; Jankovský, O. Synthesis, structure, and thermal stability of magnesium oxychloride $5\text{Mg}(\text{OH})_2 \cdot \text{MgCl}_2 \cdot 8\text{H}_2\text{O}$. *Appl. Sci.* **2020**, *10*, 1683. [[CrossRef](#)]
35. Jankovský, O.; Lojka, M.; Lauermannová, A.-M.; Antončík, F.; Pavlíková, M.; Pavlík, Z.; Sedmidubský, D. Carbon Dioxide Uptake by MOC-Based Materials. *Appl. Sci.* **2020**, *10*, 2254. [[CrossRef](#)]

